Modeling of Kinetics of Austenite-to-Allotriomorphic Ferrite Transformation in 0.37C-1.45Mn-0.11V Microalloyed Steel

C. CAPDEVILA, F.G. CABALLERO, and C. GARCÍA DE ANDRÉS

The present article is concerned with the theoretical and experimental study of the growth kinetics of allotriomorphic ferrite in medium carbon vanadium-titanium microalloyed steel. A theoretical model is presented in this work to calculate the evolution of austenite-to-allotriomorphic ferrite transformation with time at a very wide temperature range. At temperatures above eutectoid temperature, where allotriomorphic ferrite is the only austenite transformation product, the *soft-impingement* effect should be taken into account in the modeling. In that case, the Gilmour *et al.* analysis reliably predicts the progress of austenite-to-allotriomorphic ferrite transformation in this steel. By contrast, since pearlite acts as a carbon sink, the carbon enrichment of austenite due to the previous ferrite formation is avoided, and carbon concentration in austenite far from the α/γ interface remains the same as the overall carbon content of the steel. Hence, the soft-impingement effect should be neglected, and allotriomorphic ferrite is considered to grow under a parabolic law. Therefore, assumption of a semi-infinite extent austenite with constant boundary conditions is suitable for the kinetics of the isothermal decomposition of austenite. An excellent agreement (higher than 93 pct in R^2) has been obtained between the experimental and predicted values of the volume fraction of ferrite in all of the ranges of temperature studied.

I. INTRODUCTION

THE term *allotriomorphic* means that the phase is crystalline in internal structure but not in outward form. It implies that the limiting surfaces of the crystal are not regular and do not display the symmetry of its internal structure.[1,2,3] Allotriomorphic ferrite, which nucleates at the prior austenite grain boundaries, tends to grow along the austenite grain boundaries at a rate faster than in the normal direction to the boundary plane, so that its shape is strongly influenced by the presence of the grain boundaries and hence does not necessarily reflect its internal symmetry. Of course, allotriomorphic ferrite does not need to form just at austenite grain boundaries, but it invariably does so, presumably because there are no other two-dimensional heterogeneous nucleation sites in austenite more suitable.[4]

In the two last decades, many researchers have created models for the austenite-to-allotriomorphic ferrite transformation based on thermodynamic and fundamental phase transformation theory for a wide range of steels.[5,6] Unemoto *et al.*[7] developed a methodology to simulate the allotriomorphic ferrite transformation under isothermal conditions. The volume fraction of allotriomorphic ferrite was computed at every temperature using Cahn's theory for grain boundary nucleation kinetics.[8] Likewise, the Hillert–Staffanson regular solution model[9] was used to calculate thermodynamic data for several alloying elements under paraequilibrium conditions. Classical nucleation theory was applied for allotriomorphic ferrite, followed by parabolic growth kinetics. Finally, Lee *et al.*[10] developed a mathematical model for the allotriomorphic ferrite transformation in Nb microalloyed steels, considering a Fe-C-Mn-Nb system. They used the Hillert–Staffanson model to determine the austenite and ferrite carbon content at the interface and the free energy of the transformation under local and paraequilibrium conditions.

Recent works have demonstrated that medium carbon microalloyed forging steels with acicular ferrite microstructure can be manufactured at industrial scale.[11–15] The main interest of this microstructure lies in the good combination of mechanical properties that presents as compared with bainite and especially with ferritic-pearlitic microstructures. In those steels, acicular ferrite is always formed after the growth of allotriomorphic ferrite and pearlite. As a consequence, acicular ferrite transformation is inevitably influenced by previous allotriomorphic ferrite formation. The role of the allotriomorphic ferrite to promote the formation of acicular ferrite to the detriment of bainite has been reported in previous works.[16–19] Thus, the amount of acicular ferrite increases as allotriomorphic ferrite is present along the austenite grain boundaries of medium carbon microalloyed steels. Therefore, a deep understanding of the decomposition of austenite in allotriomorphic ferrite is needed in order to control the total amount of acicular ferrite present in the microstructure.

The present article is concerned with the theoretical and experimental description of the growth kinetics of allotriomorphic ferrite in medium carbon vanadium-titanium microalloyed steel in a very wide temperature range. The theoretical model presented in this work allows us to calculate the evolution of austenite-to-allotriomorphic ferrite

C. CAPDEVILA, Research Associate, formerly with the Department of Physical Metallurgy, Centro Nacional de Investigaciones Metalurgicas (CENIM), Consejo Superior de Investigaciones Cientificas (CSIC), 28040 Madrid, Spain, is with the Department of Materials Science and Metallurgy, University of Cambridge, Cambridge CB2 2QZ, United Kingdom, F.G. CABALLERO, Research Associate, and C. GARCÍA DE ANDRÉS, Senior Research Fellow, are with the Department of Physical Metallurgy, Centro Nacional de Investigaciones Metalurgicas (CENIM), Consejo Superior de Investigaciones Cientificas (CSIC).

Manuscript submitted June 12, 2000.

Table I. Chemical Composition (Weight Percent) of the Steel

C	Si	Mn	Cr	Al	Ti	V	Cu	Mo
0.37	0.56	1.45	0.04	0.024	0.015	0.11	0.14	0.025

transformation with time at temperatures at which allotriomorphic ferrite is or is not the only austenite decomposition product. This work is the continuation of previous authors' study.[20]

II. EXPERIMENTAL

The chemical composition of the steel studied is presented in Table I. The material was supplied in the form of 50-mm-square bars, obtained by conventional casting to a square ingot (2500 kg) and hot rolling to bar. Cylindrical dilatometric test pieces of 2 mm in diameter and 12 mm in length were machined parallel to the rolling direction of the bar.

The isothermal decomposition of austenite has been analyzed by means of high-resolution dilatometer (Adamel Lhomargy DT1000) described elsewhere.[21] The incubation time of allotriomorphic ferrite, or minimum time at which it is possible to find some allotriomorphs nucleated on the austenite grain boundary, is experimentally determined from dilatometric curves obtained during the isothermal decomposition of austenite. The change in length of the specimen is transmitted *via* an amorphous silica pushrod. These variations are measured by a linear variable differential transformer sensor in a gas-tight enclosure enabling testing under vacuum or an inert atmosphere with an accuracy lower than 0.1 μm, and the dilatometric curve is monitored along the thermal cycle with the help of a computer-assisted electronic device. Experimental validation of the allotriomorphic ferrite formation kinetics model developed in this work was carried out using the heating and cooling devices of the aforementioned dilatometer. The heating device consists of a very low thermal inertia radiation furnace. The power radiated by two tungsten filament lamps is focused on the specimen by means of a bi-elliptical reflector. The temperature is measured with a 0.1-mm-diameter chromel-alumel (type K) thermocouple welded to the specimen. Cooling is carried out by blowing a jet of helium gas directly onto the specimen surface. The helium flow rate during cooling is controlled by a proportional servovalve. These devices ensure an excellent efficiency in controlling the temperature and holding time of isothermal treatments as well as fast cooling in quenching processes.

As is well known, prior austenite grain size (PAGS) exerts an important influence on the decomposition of austenite.[22,23] The PAGS parameter directly affects the growth kinetics of allotriomorphic ferrite obtained by isothermal decomposition of the austenite. But, there is no influence on the nucleation time of this phase.[24,25] In this sense, austenitization conditions were fixed to avoid the influence of the austenite grain size on the kinetics of allotriomorphic ferrite formation and to study specifically the effect of the isothermal decomposition temperature on the growth kinetics of this phase. Since the growth rate of allotriomorphs is higher the finer the PAGS, a coarse PAGS of 76 μm was selected to make the experimental study of the growth kinetics of allotriomorphic ferrite easier. Thus, specimens were austenitized at 1523 K for 1 minute and subsequently isothermally transformed at 973, 913, and 873 K during different times. In order to freeze the microstructure at those temperatures, specimens were quenched to room temperature by helium gas flow at a cooling rate of 200 K/s.

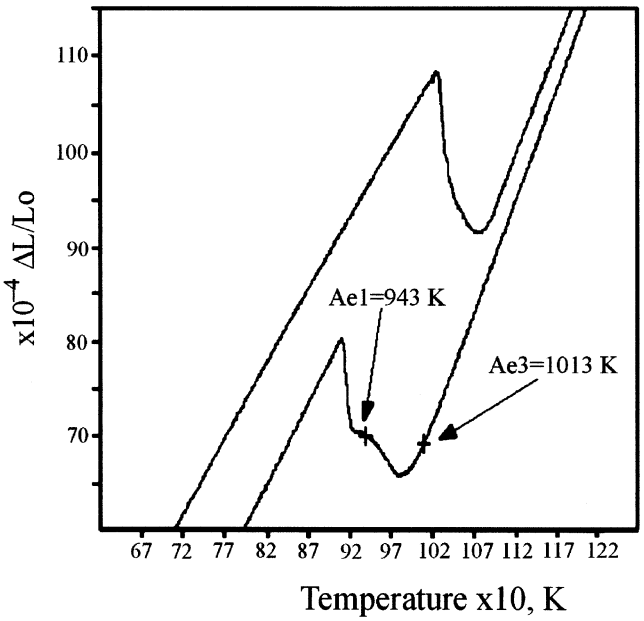

Fig. 1—Ae_3 and Ae_1 critical temperatures marked on the cooling segment of a dilatometric curve obtained by continuous cooling at 0.05 K/s.

Specimens were polished in the usual way for metallographic examination. Nital-2 pct etching solution was used to reveal the ferrite microstructure by optical microscopy. The PAGS was estimated on micrographs by counting the number of grains intercepted by straight lines long enough to yield at least 50 intercepts in total. The effects of a moderately nonequiaxial structure may be eliminated by counting the intersections of lines in four or more orientations covering all the observation fields with an approximately equal weight.[26] Moreover, the volume fraction of allotriomorphic ferrite (V_α) was statistically estimated by a systematic manual point counting procedure.[26] A grid superimposed on the microstructure provides, after a suitable number of placements, an unbiased statistical estimation of the V_α.

The austenite-to-allotriomorphic ferrite (Ae_3) and austenite-to-pearlite (Ae_1) critical temperatures were experimentally determined by dilatometric and metallographic analysis. Initially, both temperatures were estimated from a dilatometric curve obtained by continuous cooling at a rate of 0.05 K/s. This is the rate normally used for considering quasi-equilibrium conditions.[27] Subsequently, those critical points were verified by interrupted cooling by quenching tests and metallographic examination of the obtained microstructure. Figure 1 shows both critical temperatures marked on the dilatometric curve (Ae_3 = 1013 K and Ae_1 = 943 K).

The equilibrium volume fraction of allotriomorphic ferrite

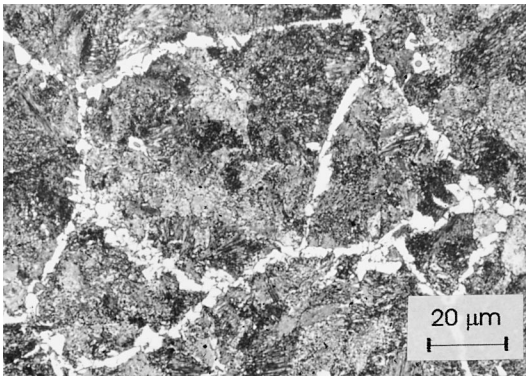

(*a*)

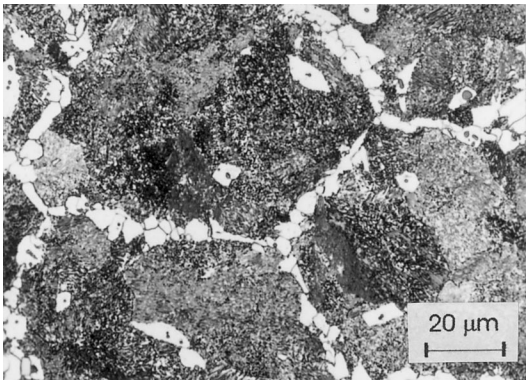

(*b*)

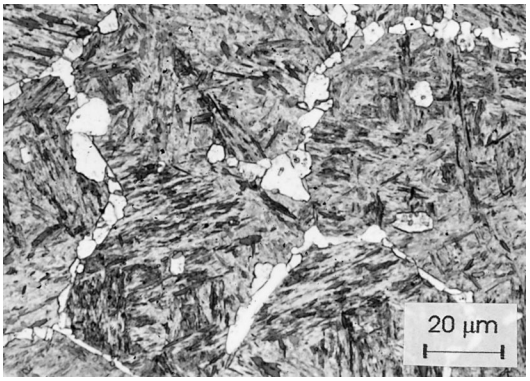

(*c*)

Fig. 2—Microstructures obtained after isothermal heat treatment during 10 h at (*a*) 973 K, (*b*) 913 K, and (*c*) 873 K. (M is martensite, F is ferrite, and P is pearlite.)

(*Ve*) formed during the isothermal decomposition of austenite at each temperature tested was again determined by a combination of dilatometric and metallographic analysis. For the three studied temperatures, the dilatometric curve (relative change of length ($\Delta L/Lo$) *vs* time (t)) reaches saturation at holding times lower than 10 hours. Then, isothermal heat treatments for 10 hours allowed measurement of (*Ve*) at the three studied temperatures. Figure 2 shows the quenching microstructures obtained after the complete isothermal decomposition of austenite at 973, 913, and 873 K. Table II lists the experimental values of *Ve*. As this table shows, for temperatures below Ae_1, the total amount of allotriomorphic ferrite decreases as isothermal temperature decreases.

Table II. Equilibrium Allotriomorphic Ferrite Volume Fraction

Temperature, K	*Ve*, Pct
973	23
913	28
873	18

Table III. Calculated Values of $\xi(\theta)$, D_C^γ, ΔG_ν, and a Parameters

T, K	$\xi(\theta)$	$D_C^\gamma \times 10^{-14}$, $m^2\ s^{-1}$	$\Delta G_\nu \times 10^{7}$, $J\ m^{-3}$	$\alpha \times 10^{-10}$, m
973	0.009	30.9	−0.96	3.306
913	0.016	12.0	−3.68	3.302
873	0.023	5.8	−5.94	3.300

III. RESULTS AND DISCUSSION

A. *Incubation Time of Allotriomorphic Ferrite*

Lange *et al.*[28] proposed a model to calculate the classical nucleation rate of allotriomorphic ferrite based on a traditional disk-shaped "pillbox" nucleus. In that case, the incubation time for allotriomorphic ferrite is estimated as

$$\tau = \frac{12 k_B T a^4 \sigma_{\alpha\gamma}}{D_C^\gamma \bar{x} \nu_\alpha^2 \Delta G_\nu^2} \qquad [1]$$

where k_B is the Boltzmann constant; D_C^γ is the diffusivity of carbon in austenite; ν_α is the volume of an atom of iron in ferrite; a is the average of the lattice parameters of both phases, ferrite and austenite; $\bar{x}$ is the average carbon content in mole fraction; ΔG_ν is the volume free energy change associated with the formation of the nucleus; $\sigma_{\alpha\gamma}$ is the interfacial energy of a disorder ferrite; and T is the isothermal temperature.

The theoretical determination of D_C^γ, due to Siller and McLellan[29] and reviewed by Bhadeshia,[30] considers both the kinetic and equilibrium thermodynamic behavior of carbon in austenite. Calculations of D_C^γ also take into account the concentration dependence of the activity of carbon in austenite, and the repulsive interactions between the nearest neighboring carbon atoms located in octahedral interstitial sites. Thus, the diffusivity D_C^γ is calculated by two factors: one of them is a concentration-dependent factor and the other one is independent:

$$D_C^\gamma = \xi(\theta) \frac{k_B T}{h} \left(\frac{\lambda^2}{3\gamma_m}\right) \exp\left\{-\frac{\Delta G^*}{k_B T}\right\} \qquad [2]$$

where $\xi(\theta)$ is the carbon concentration–denpendent factor obtained according to Bhadeshia's calculations[30] and takes the values listed in Table III; ΔG^* is the activation free energy for diffusion, which is independent of composition and temperature; γ_m is an activity coefficient assumed constant; λ is the distance between the {002} austenite planes; and h is the Planck's constant. Bhadeshia[30] found that $\Delta G^*/k_B$ = 21,230 K and $\ln(\gamma_m/\lambda^2)$ = 31.84. The values of D_C^γ for temperatures ranging from 973 to 873 K are also listed in Table III.

The volume free energy change, ΔG_ν, in Eq. [1] has been

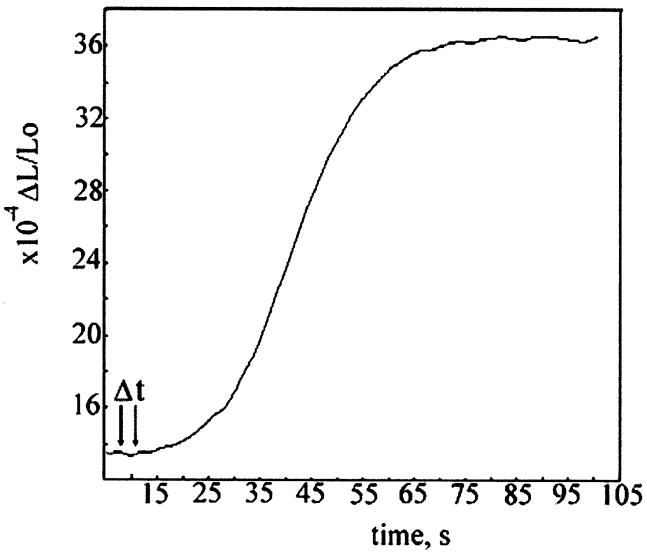

Fig. 3—Dilatometric curve (relative change in length *vs* time) obtained during isothermal decomposition of austenite at 873 K during 100 s for the studied steel.

calculated with the help of commercial software denominated MTDATA,[31] which contains a large and rigorously evaluated thermodynamic database. The ΔG_ν calculations take into account the effect of all the alloying elements in the decomposition of austenite. The values obtained for the studied steels are listed in Table III. The value of α in Eq. [1] has been calculated considering the influence of different alloying elements on ferrite and austenite lattice parameters. The ferrite lattice parameter has been calculated using the relations given by Bhadeshia,[32] whereas the austenite lattice parameter has been calculated as reported by Ridley *et al.*[33] and Dyson and Holmes.[34] The values of α at temperatures ranging from 973 to 873 K are listed in Table III. Likewise, a $\sigma_{\alpha\gamma}$ value of 0.705 J m^{-2}[28,35] and $\nu_\alpha = 8.785 \times 10^{-30}$ m^3[36] have been considered in Eq. [1] for τ calculations.

The experimental determination of incubation time has been carried out by dilatometry and metallography. The experimental incubation time is defined as the minimum time at which it is possible to find some allotriomorphs nucleated on the austenite grain boundary. A detailed analysis of the dilatometric curve associated with the isothermal decomposition of austenite (Figure 3) allows determination of an interval of time, Δt, in which it is more likely to find the incubation time. With the aim of carrying out an accurate determination, samples were isothermally treated at different holding times within the Δt interval and immediately quenched. A metallographic analysis of those samples determined the incubation time at which some allotriomorphs appear in the microstructure. Figure 4 shows an example of a microstructure with allotriomorphs at the initial stage of their formation.

Figure 5 shows a comparison between calculated (dashed line) and experimental (points) incubation time values for the studied steel. It can be concluded from this figure that calculated results for the incubation time are in good agreement with the predicted values from calculations proposed in this work.

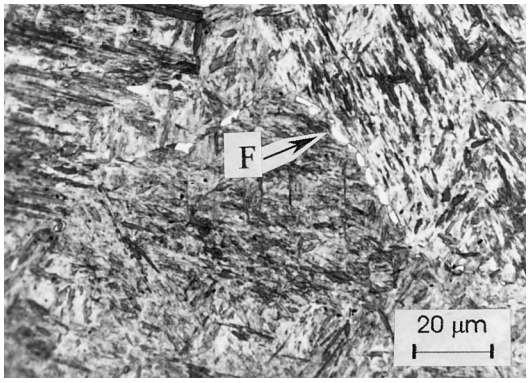

Fig. 4—Optical micrograph of studied steel after isothermal heat treatment at 913 K during 18 s.

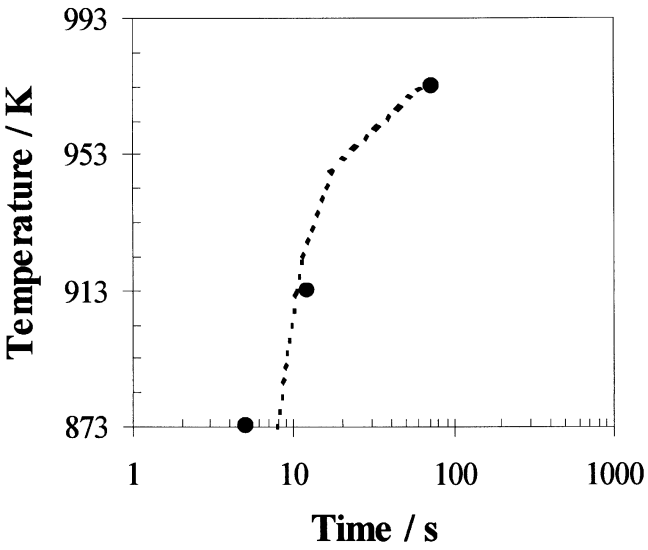

Fig. 5—Experimental and calculated results for the incubation time of isothermally formed allotriomorphic ferrite.

B. *Kinetics of Austenite-to-Allotriomorphic Ferrite Transformation*

After nucleation occurs at the austenite grain boundaries, the thin layers of ferrite that decorate the austenite grain boundaries thicken at a rate controlled mainly by the diffusion of carbon in the austenite ahead of the advancing ferrite/austenite interface.[37] The half-thickness of the allotriomorphs, *Z*, is generally calculated under parabolic growth conditions according to the following expression:[38]

$$Z = \alpha_1 t^{1/2} \qquad [3]$$

where α_1 is the one-dimensional parabolic growth rate constant and t is the growth time. The value of α_1 can be obtained by numerical solution from the equation:[39]

$$\alpha_1 \exp\left(\frac{\alpha_1^2}{4D_C^\gamma}\right) \operatorname{erfc}\left(\frac{\alpha_1}{2\sqrt{D_C^\gamma}}\right) = 2\left(\frac{D_C^\gamma}{\pi}\right)^{1/2} \frac{C^{\gamma\alpha} - \overline{C}}{C^{\gamma\alpha} - C^{\alpha\gamma}} \qquad [4]$$

where D_C^γ is the diffusivity of carbon in austenite, $\overline{C}$ is the overall carbon content, $C^{\gamma\alpha}$ is the austenite solute content

Table IV. Calculated Values of $C^{\alpha\gamma}$, $C^{\gamma\alpha}$, and α_1

T, K	$C^{\alpha\gamma}$, Wt Pct	$C^{\gamma\alpha}$, Wt Pct	$\alpha_1 \times 10^{-7}$, m $s^{-1/2}$
973	0.014	0.500	2.88
913	0.016	0.903	4.85
873	0.016	1.195	4.76

at the interface, and $C^{\alpha\gamma}$ is the ferrite solute content at the interface.

According to Bhadeshia,[40] the consideration of *paraequilibrium* is a good approach for the kinetics of this transformation. In that case, partitioning of substitutional solute atoms does not have time to occur and the adjoining phases have identical X/Fe atom ratios, where X represents the substitutional solute elements. Then, the substitutional lattice is configurationally frozen, but interstitial solutes such as carbon are able to partition and attain equilibration of chemical potential in both phases. Hence, the values of $C^{\gamma\alpha}$ and $C^{\alpha\gamma}$ in Eq. [4] refer to carbon concentrations and they were calculated according to the procedure reported by Shiflet *et al.*[41] The $C^{\gamma\alpha}$ and $C^{\alpha\gamma}$ values as well as the α_1 values are listed in Table IV.

1. *Kinetics of allotriomorphic ferrite formation at $T > Ae_1$*

At temperatures where allotriomorphic ferrite is the only austenite decomposition product, overlapping of carbon diffusion gradients occurs due to allotriomorphs growing from opposite sides of a grain. This effect, known as *soft impingement*, should be taken into account in the modeling of the growth kinetics of allotriomorphic ferrite. Soft impingement is considered in the model using an analytical treatment based on the work by Gilmour *et al.*[42]

The one-dimensional growth of planar grain boundary allotriomorphs from opposite sides of an austenite grain is illustrated schematically in Figure 6(a). This process may be considered in two stages. The first stage involves a parabolic growth from both sides of the grain according to the assumption that austenite has a semi-infinite extent with constant boundary conditions. In this stage, the carbon concentration in austenite far from the α/γ interface remains the same as the overall carbon content of the steel. During the second stage, soft impingement occurs, the growth rate considerably decreases, and the austenite is considered to have a finite extent beyond the α/γ interface. Therefore, the carbon concentration in the center of the austenite grain is given by balancing the amount of carbon enrichment of the austenite against the corresponding depletion of the ferrite.[40,43] Figure 6(b) shows a scheme of the carbon concentration profiles in austenite (dark lines) during the soft-impingement stage. The carbon concentration in ferrite has been considered constant and negligibly small ($C^{\alpha\gamma} = 0$) (dark in X-axis). It is assumed that the α/γ interface moves in the z direction normal to the interface plane, and austenite is considered to have a finite size L in that direction. The position of the interface at any time t is defined by $z = Z$, being $Z = 0$ at $t = 0$. In this initial state, the carbon concentration in the austenite is uniform and corresponds to the overall carbon composition ($\overline{C}$). The position of the interface at the onset of soft impingement is defined by $z = Z_1$ and $t = t_1$. At that moment, carbon concentration rises at every point in the austenite located ahead of the interface. At a subsequent

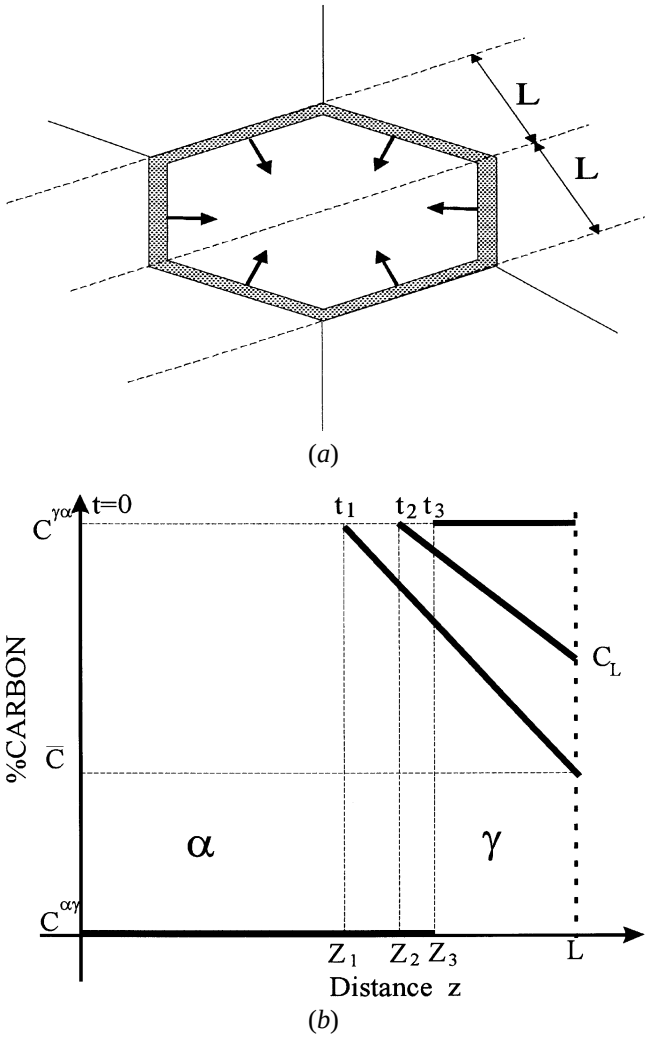

Fig. 6—Diagram illustrating the soft-impingement process: (*a*) schematic representation of the growth of grain boundary allotriomorphs and (*b*) carbon concentration profile for the calculation of impingement time. The dark lines represent the carbon profile in austenite and ferrite.

stage ($z = Z_2$ and $t = t_2$), the concentration of carbon in the center of the austenite grain increases from $\overline{C}$ to C_L. Finally, when $z = Z_3$ and $t = t_3$, the carbon content in austenite is uniform and equal to that of austenite in the α/γ interface ($C^{\gamma\alpha}$).

At the onset of the soft impingement, when the position of the interface is $z = Z_1$, the carbon enrichment of the austenite is equal to the amount of carbon removed from the ferrite. Therefore, according to Figure 6(b), the mass balance allows calculation of the position of the interface Z_1, which is given by

$$Z_1 = \frac{L(C^{\gamma\alpha} - \overline{C})}{(C^{\gamma\alpha} + \overline{C})} \qquad [5]$$

where L is the semiextent of the austenite grain. Likewise, the position of the interface Z_3 when the carbon activity becomes uniform is calculated using the appropriate mass balance, and it is expressed as follows:

$$Z_3 = L\left(1 - \frac{\overline{C}}{C^{\gamma\alpha}}\right) \qquad [6]$$

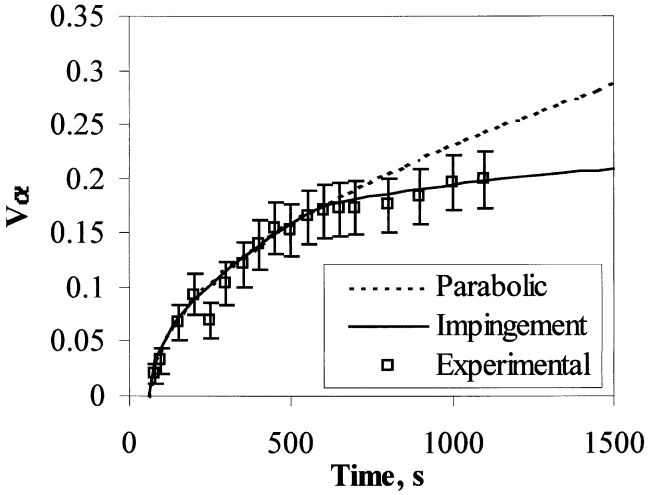

Fig. 7—Comparison between measured and calculated V_α values under parabolic and impingement considerations during the isothermal decomposition of austenite at 973 K.

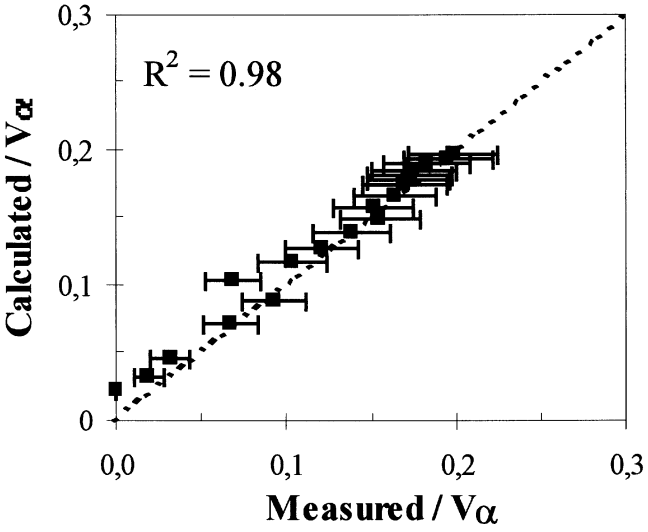

Fig. 8—A comparison of the experimental and predicted ferrite volume fraction formed at a temperature higher than Ae_1. Soft impingement is considered in calculations.

On the other hand, the carbon concentration in the center of the austenite grain (C_L) can also be calculated also by balancing the amount of carbon enrichment of austenite against the carbon depletion in the ferrite at an intermediate position Z_2 (Figure 6(b)) during the soft-impingement process ($Z_1 < Z_2 < Z_3$):

$$C_L = \frac{2L\overline{C} - C^{\gamma\alpha} \cdot (L - Z_2)}{L - Z_2} \quad [7]$$

The instantaneous interfacial carbon mass balance is described as follows:

$$C^{\gamma\alpha} \frac{dZ_2}{dt} = -D_C^{\gamma} \frac{dC}{dz} \quad [8]$$

where dC/dz represents the gradient of carbon ahead of the interface. Figure 6(b) shows that in position $z = Z_2$, this gradient can be expressed by

$$\frac{dC}{dz} = -\frac{C^{\gamma\alpha} - C_L}{L - Z_2} \quad [9]$$

Finally, combining Eqs. [7] through [9], the following differential equation is obtained:

$$\frac{dZ_2}{dt} = \frac{2D_C^{\gamma}(Z_3 - Z_2)}{(L - Z_2)^2} \quad [10]$$

This velocity expression may then be integrated to yield the interface position (*i.e.*, thickness of ferrite) as a function of time during isothermal decomposition of austenite. In the one-dimensional model, the calculated volume fraction of allotriomorphic ferrite can be then approximated as

$$V_\alpha = \frac{z}{L}; \quad (z = Z_2) \quad [11]$$

According to Eqs. [6] and [11] with $z = Z_3$, a maximum volume fraction of 26 pct is obtained during the isothermal decomposition of austenite into ferrite at 973 K, which is in excellent agreement with the experimental value listed in Table II. Figure 7 shows the calculated and measured V_α values under parabolic and soft-impingement growth conditions. This figure suggests that care needs to be taken with the assumption of semi-infinite austenite grain extent and the modeling of allotriomorphic ferrite transformation under parabolic growth conditions in medium carbon microalloyed steels. It can be concluded that the soft-impingement effect should be considered in the study of allotriomorphic ferrite growth kinetics of this steel. From Figure 8, it is concluded that a great overall level of agreement between experiment and theory exists as soft-impingement growth conditions are considered in calculations. Points lying on the line of unit slope show a perfect agreement between experimental and calculated values. The term R^2 in Figure 8 is the square correlation factor of the experimental and calculated volume fraction of ferrite and quantifies the accuracy of the calculations. The accuracy of the model is 98 pct, which can be considered excellent for a thermodynamic and kinetics model.

2. *Kinetics of allotriomorphic ferrite formation at $T < Ae_1$*

At temperatures lower than Ae_1, the isothermal decomposition of austenite yields a ferrite-pearlite final microstructure. Pearlite is a lamellar product of eutectoid decomposition. A pearlite nodule is composed of multiple colonies; each colony has parallel lamellae of ferrite and cementite, which are orientated differently with respect to lamellae in adjacent colonies. The austenite transforms into pearlite by a reconstructive mechanism at temperatures below the eutectoid temperature Ae_1. The formation of allotriomorphic ferrite enriches the surrounding austenite in carbon, promoting the formation of cementite nucleus at the α/γ interface, and the local reduction of carbon content in the austenite that surrounds the cementite nucleus leads to the ferrite formation of pearlite aggregate. The simultaneous ferrite and cementite formation process yields the characteristic lamellar structure of pearlite.[3] As soon as pearlite surrounds a ferrite allotriomorph, its growth will finish, as is shown in Figure 9. In addition, the carbon enrichment of austenite due to allotriomorphic ferrite formation is avoided,

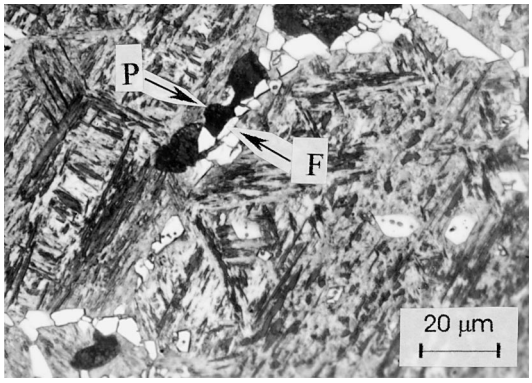

Fig. 9—Early stage of pearlite transformation during the isothermal decomposition of austenite at 913 K during 60 s.

and carbon concentration in austenite far from the α/γ interface remains the same as the overall carbon content of the steel. Hence, the soft-impingement effect can be neglected. Allotriomorphic ferrite is considered to grow under a parabolic law, and the assumption of a semi-infinite extent austenite with constant boundary conditions is suitable for the kinetics of the isothermal decomposition of austenite at temperatures below Ae_1.

Reed and Bhadeshia[44] proposed the following equation to describe the evolution of V_α with time ($t > \tau$) during the isothermal decomposition of austenite, assuming site saturation for nucleation of ferrite in austenite grain boundaries and within the framework of Johnson–Mehl–Avrami heterogeneous transformation kinetics theory:

$$V_\alpha = V_e\left[1 - \exp\left(-\frac{2S_v\alpha_1(t-\tau)^{1/2}}{\phi}\right)\right] \qquad [12]$$

where t is the isothermal holding time; τ is the incubation time calculated according to Eq. [1]; α_1 is the one-dimensional parabolic rate constant; S_V is the austenite grain surface per unit volume; V_e is the equilibrium volume fraction of allotriomorphic ferrite; and ϕ is the supersaturation in carbon, which can be estimated from the phase diagram as follows:

$$\phi = \frac{\overline{C} - C^{\gamma\alpha}}{C^{\alpha\gamma} - C^{\gamma\alpha}} \qquad [13]$$

Assuming austenite grains to be tetrakaidecahedra, S_V in Eq. [12] can be expressed in terms of the average austenite grain diameter d_γ by[8]

$$S_V = \frac{3.35}{d_\gamma} \qquad [14]$$

with $d_\gamma = 2L$ (Figure 6(a)).

Figure 10 shows the experimental and predicted evolution of V_α during the isothermal decomposition of austenite at 913 and 873 K. Likewise, Figure 11 shows in more detail the V_α values corresponding to the beginning of the allotriomorphic ferrite transformation at both temperatures. From both figures, it is concluded that the lower the ferrite formation temperature, the slower allotriomorphic ferrite grows. That behavior is consistent with the lower temperature, lower carbon mobility in austenite. A comparison of the calculated and experimental V_α values for $T < Ae_1$ is shown in Figure 12. This figure suggests that a good agreement (93 pct in R^2) between experiment and theory exists in the calculations.

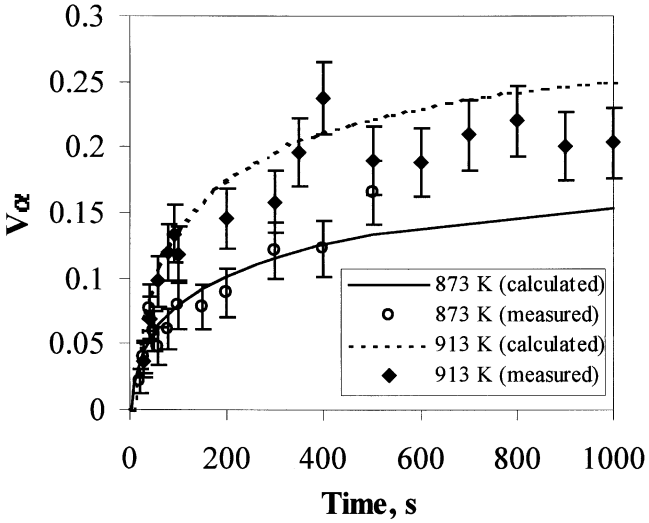

Fig. 10—Comparison between calculated and measured V_α values during the isothermal decomposition of austenite at 913 and 873 K.

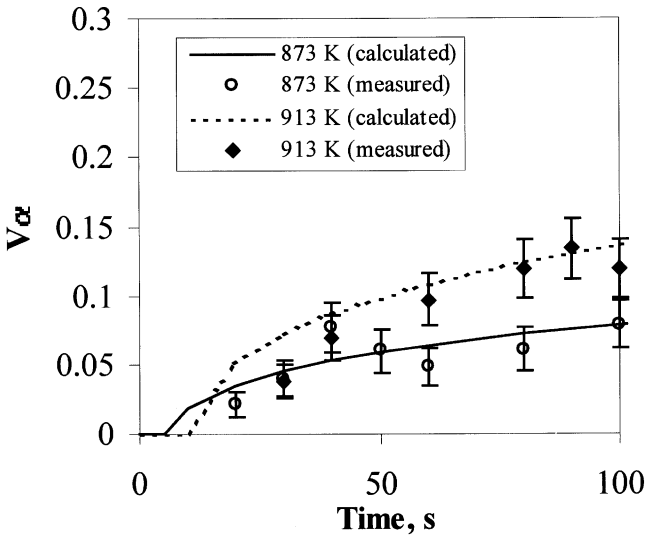

Fig. 11—Comparison between calculated and measured V_α values at the initial stages of isothermal decomposition of austenite in allotriomorphic ferrite at 913 and 873 K.

Finally, it is worth mentioning that this model is based on physical and metallurgical principles of phase transformations. Although the proposed model has only been validated for a 0.37C-1.45Mn-0.11V steel, in principle, this model is able to predict the isothermal decomposition of austenite for a wide range of steels. This model is different from those empirical and semiempirical models created by fitting equations to experimental data.

IV. CONCLUSIONS

1. The kinetics of austenite-to-allotriomorphic ferrite transformation has been described in a wide temperature range for a 0.37C-1.45Mn-0.11V (in wt pct) microalloyed steel.

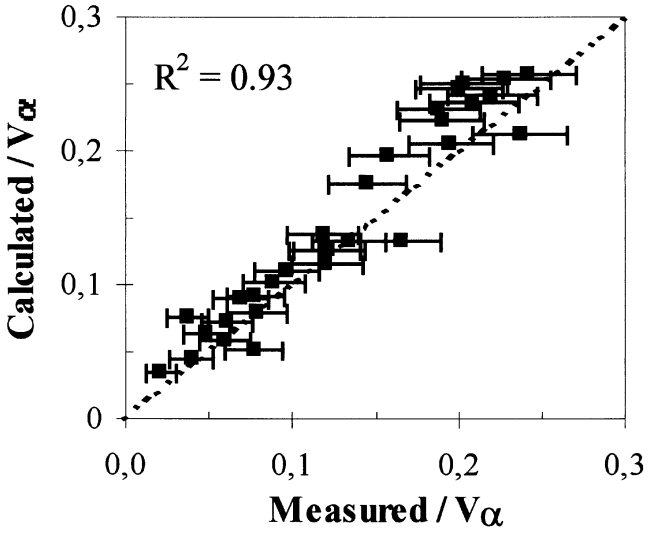

Fig. 12—A comparison of the experimental and predicted ferrite volume fraction formed at a temperature lower than Ae_1.

Since the austenite decomposition products at temperatures above and below Ae_1 are different, two different mathematical models have been proposed for the isothermal austenite decomposition in allotriomorphic ferrite.

2. A mathematical process to calculate the incubation time for the isothermal formation of allotriomorphic ferrite has been described. Experimental validation of calculations has been carried out using dilatometric and metallographic analysis. An excellent agreement between calculated and measured incubation time values for the isothermal formation of allotriomorphic ferrite has been found for the studied steel.
3. Gilmour *et al.* analysis considering the soft-impingement effect gives a very good representation of the kinetics of austenite-to-allotriomorphic ferrite transformation at temperatures above Ae_1 in the studied steel. An excellent agreement (98 pct in R^2) has been obtained between experimental and predicted values of volume fraction of allotriomorphic ferrite.
4. Since pearlite is formed at temperatures below Ae_1, the soft-impingement effect should be neglected for the austenite-to-allotriomorphic ferrite transformation kinetics. In that case, Reed and Bhadeshia analysis considering the growth of allotriomorphic ferrite under a parabolic law is the most suitable representation of allotriomorphic ferrite transformation kinetics. A very good agreement (93 pct in R^2) between calculated and measured volume fractions of allotriomorphic ferrite has been found at those temperatures.

ACKNOWLEDGMENTS

The authors acknowledge financial support from the Spanish Comisión Interministerial de Ciencia y Tecnologia (CICYT) (Project-PETRI 95-0089-OP). GSB Acero S.A and CEIT are thanked for providing the steel and for their collaboration in this project.

REFERENCES

1. H.I. Aaronson: *Symp. on the Mechanism of Phase Transformations in Metals*, Institute of Metals, London, 1955, p. 47.
2. C.A. Dube, H.I. Aaronson, and R.F. Mehl: *Rev. Metall.*, 1958, vol. 3, pp. 201-10.
3. J.W. Christian: *Theory of Phase Transformation and Alloys*, 2nd ed., Pergamon Press, Oxford, United Kingdom, 1975, Part 1, p. 10.
4. H.K.D.H. Bhadeshia: in *Mathematical Modelling of Weld Phenomena III*, H. Cerjak and H.K.D.H. Bhadeshia, eds., Institute of Materials, London, 1996, pp. 1-50.
5. H.K.D.H. Bhadeshia, L.-E. Svensson, and B. Gretoft: *Proc. Conf. on Welding Metallurgy of Structural Steels*, J.Y. Koo, ed., TMS-AIME, Warrendale, PA, 1987, pp. 517-30.
6. G.P. Krielaart, M. Onik, C.M. Brakman, F.D. Tichelaar, E.J. Mittemeijer, and S. van der Zwaag: *Z. Metallkd.*, 1994, vol. 84, pp. 756-65.
7. M. Unemoto, A. Hiramatsu, A. Moriya, T. Watanabe, S. Nanaba, N. Nakajima, G. Anan, and Y. Higo: *Iron Steel Inst. Jpn. Int.*, 1992, vol. 32, pp. 306-15.
8. J.W. Cahn: *Acta Metall.*, 1956, vol. 4, pp. 449-59.
9. M. Hillert and L.I. Staffanson: *Acta Chem. Scand.*, 1970, vol. 24, pp. 3618-26.
10. K.L. Lee, J.K. Lee, K.B. Kang, and O. Kwon: *Iron Steel Inst. Jpn. Int.*, 1992, vol. 32, pp. 326-34.
11. I. Madariaga, I. Gutierrez, C. Garcia de Andres, and C. Capdevila: *Scripta Metall. Mater.*, 1999, vol. 41, pp. 229-35.
12. I. Madariaga and I. Gutierrez: *Acta Mater.*, 1999, vol. 47, pp. 951-60.
13. I. Madariaga, I. Gutiérrez, and J.L. Romero: *Metall. Mater. Trans. A*, 1998, vol. 29A, pp. 1003-15.
14. M.A. Linaza, J.L. Romero, J.M. Rodriguez-Ibabe, and J.J. Urcola: *Scripta Metall.*, 1993, vol. 29, p. 1217.
15. I. Madariaga and I. Gutiérrez: *Scripta Metall. Mater.*, 1997, vol. 37, pp. 1185-92.
16. C. García De Andrés, C. Capdevila, and F.G. Caballero: *Proc. Congreso Nacional de Tratamientos Térmicos y de Superficie TRATERMAT 98*, M. Carsi, F. Peñlba, O.A. Ruano and B.J. Fernández, CENIM-CSIC, Madrid, 1998, p. 135.
17. H.K.D.H. Bhadeshia: *Mater. Sci. Technol.*, 1985, vol. 1, p. 497.
18. S.S. Babu, H.K.D.H. Bhadeshia, and L.-E. Svensson: *J. Mater. Sci. Lett.*, 1991, vol. 10, p. 142.
19. S.S. Babu and H.K.D.H. Bhadeshia: *Mater. Sci. Technol.*, 1990, vol. 6, p. 1005.
20. C. García de Andrés, C. Capdevila, and F.G. Caballero, and H.K.D.H. Bhadeshia: *Scripta Mater.*, 1998, vol. 39, pp. 853-59.
21. C. García de Andrés, G. Caruana, and L.F. Alvarez: *Mater. Sci. Eng.*, 1998, vol. A241, p. 211.
22. J. Bardford and W.S. Owen: *J. Iron Steel Inst.*, 1961, vol. 197, p. 146.
23. A.K. Sinha: *Ferrous Physical Metallurgy*, Butterworths, Boston, MA, 1989, p. 379.
24. K.C. Russell: *Acta Metall.*, 1968, vol. 16, p. 761.
25. H.K.D.H. Bhadeshia: *Met. Sci.*, 1982, vol. 16, p. 159.
26. G.F. Vander Voort: *Metallography. Principles and Practice*, McGraw-Hill, New York, NY, 1984, p. 27.
27. C. García, L.F. Alvarez, and M. Carsí: *Weld. Int.*, 1982, vol. 6, p. 612.
28. W.F. Lange, M. Enomoto, and H.I. Aaronson: *Metall. Trans. A*, 1988, vol. 19A, pp. 427-40.
29. R.H. Siller and R.B. McLellan: *Metall. Trans. A*, 1970, vol. 1, pp. 985-88.
30. H.K.D.H. Bhadeshia: *Met. Sci.*, 1981, vol. 15, p. 477.
31. S.M. Hodson: *MTDATA—Metallurgical and Thermomechanical Databank*, National Physical Laboratory, Teddington, United Kingdom, 1989, p. 1.
32. H.K.D.H. Bhadeshia: *Materials Algorithms Project (MAP)*, URL: www.msm.cam.ac.uk/map/steel/subs/ferr-b.html.
33. N. Ridley, H. Stuart, and L. Zwell: *Trans. AIME*, 1969, vol. 245, p. 1834.
34. D.J. Dyson and B. Holmes: *J. Iron Steel Inst.*, 1970, vol. 208, p. 469.
35. N.A. Gjostein, H.A. Domian, H.I. Aaronson, and E. Eichen: *Acta Metall.*, 1966, vol. 14, p. 1637.
36. R.W.K. Honeycombe and H.K.D.H. Bhadeshia: *Steels: Microstructure and Properties*, Edward Arnold, London, 1995, p. 5.
37. C. Atkinson, H.B. Aaron, K.R. Kinsman, and H.I. Aaronson: *Metall. Trans. A*, 1973, vol. 4, pp. 783-92.
38. C. Zener: *J. Appl. Phys.*, 1949, vol. 20, p. 950.
39. J.W. Christian: *Theory of Transformations in Metals and Alloys*, 2nd ed., Pergamon, Oxford, United Kingdom, 1975, Part I, p. 482.

40. H.K.D.H. Bhadeshia: *Progr. Mater. Sci.*, 1985, vol. 29, p. 321.
41. G.J. Shiflet, J.R. Bradley, and H.I. Aaronson: *Metall. Trans. A*, 1978, vol. 9A, pp. 999-1008.
42. J.B. Gilmour, G.R. Purdy, and J.S. Kirkaldy: *Metall. Trans. A*, 1972, vol. 3, pp. 3213-22.
43. C. Capdevila, C. Garcia de Andres, and H.K.D.H. Bhadeshia: *Materials Algorithms Project (MAP)*, URL: www.msm.cam.ac.uk/map/steel/programs/ferr-b.html.
44. R.C. Reed and H.K.D.H. Bhadeshia: *Mater. Sci. Technol.*, 1992, vol. 8, p. 421.